ISSN 1560-0904, Polymer Science, Ser. B, 2015, Vol. 57, No. 6, pp. 717–729. © Pleiades Publishing, Ltd., 2015.

COMPOSITES

Microwave-Induced Chemical Functionalization of Carboxylated Multi-Walled Nanotubes with *p*-Aminophenol: Towards the Synthesis of MWCNT–Poly(amide-imide) Hybrids[1]

S. Mallakpour[a,b,c] and A. Zadehnazari[a]

[a] *Organic Polymer Chemistry Research Laboratory, Department of Chemistry, Isfahan University of Technology, Isfahan, 84156-83111, Iran*

[b] *Nanotechnology and Advanced Materials Institute, Isfahan University of Technology, Isfahan, 84156-83111, Iran*

[c] *Center of Excellence in Sensors and Green Chemistry, Department of Chemistry, Isfahan University of Technology, Isfahan, 84156-83111, Iran*

e-mail: mallak@cc.iut.ac.ir, mallakpour84@alumni.ufl.edu, mallak777@yahoo.com

Received July 6, 2015;
Revised Manuscript Received, August 27, 2015

Abstract—Covalent functionalization of multi-walled carbon nanotubes (MWCNT) with *p*-aminophenol was conducted to give enhanced solubility and dispersability by rapidly and efficiently generating of an appreciable amount of hydrophilic functional groups using microwave radiation. The functionalized MWCNTs were analyzed by means of field emission and transmission electron microscopy, Fourier transform infrared spectroscopy, X-ray diffraction, and thermogravimetric analysis. The surface-modified MWCNTs showed better chemical stability in common solvents. The functionalized MWCNT/poly(amide-imide) hybrid films prepared by solution blending method showed a good thermal stability and an increase in the elastic modulus with increasing of functionalized MWCNT content.

DOI: 10.1134/S1560090415070040

INTRODUCTION

The recent discovery of carbon nanotubes (CNTs) has led to a great amount of research on improving the macroscopic properties of polymers by incorporating the nanotubes into the polymer matrix [1, 2]. CNTs are stronger and lighter than steel, while also having dimensions smaller than current fillers for nanocomposites. They have unique structural, mechanical, thermal and electrical properties that make them attractive for different engineering applications [3–5]. However, while CNT composites have shown great promise, the inherent tendency to agglomerate has limited their successful application as nanoscale filler. Due to the fact that CNTs are difficult to disperse with conventional polymer processing methods, new approaches have been developed to increase dispersion and reproducibility. Melt mixing, solution processing, in-situ polymerization and polymer grafting have all been used as techniques to adequately disperse nanotubes within a polymer matrix [6–10]. Solution blending is a valuable technique for both nanotube dispersion and composite formation, but it is less suitable for industrial scale processes. The melt mixing is preferred because of its speed and simplicity. The major advantage of this method is that no solvent is employed to disperse CNTs. Melt blending uses a high temperature and a high shear force to disperse CNTs in a polymer matrix, and is most compatible with current industrial practices. Compared with the solution mixing methods, this technique is generally considered less effective to disperse CNTs in polymers than that of solution mixing, and its application is also limited to low filler concentrations in thermoplastic matrices. The main advantage of in-situ polymerization being the creation of a covalent bond between the tube and the matrix [2, 3, 6]. Recently, surface modification of nanotubes has been performed in order to aid dispersion. Functionalization and solubilization are important aspects of the chemistry of CNTs, these chemical manipulations being essential for many of the applications of CNTs especially good dispersion in the polymer matrices [11]. Compared to the aforementioned techniques, chemical functionalization and polymer grafting can help stabilizing the dispersion, since it can prevent reaggregation of CNTs, allowing coupling them with a polymeric matrix. Unfortunately, the resulting nanocomposites have all performed well below theoretical predictions. Therefore, current research is aimed not only at developing methods to disperse nanotubes adequately, but also to understand the nature of the interface between the polymer and the nanotubes, and its influence on bulk performance [12, 13]. Surface modification, in general, thus leads not only to placing a given group on the CNT outer

[1] The article is published in the original.

surface but also to creating some type of surface defect. However, in order to improve solubility and dispersability in solutions or matrices, processing, and selective binding affinity to target materials, these carbon nanomaterials need to be surface-functionalized with organic molecules. Functionalization approaches can be divided into chemical (covalent) and physical (non-covalent) functionalization as interactions between active materials and CNTs [14–16]. Chemical functionalization is based on the covalent bond of functional groups onto carbon form of CNTs. It can be performed at the end caps of nanotubes or at their sidewalls, which have many defects. Direct covalent sidewall functionalization is associated with a change of hybridization from sp^2 to sp^3 and a simultaneous loss of p-conjugation system on graphene layer. This process can be realized by reaction with some molecules of a high chemical reactivity. Various methods were used for this purpose [17]. Another method is defect functionalization of CNTs. These intrinsic defects are supplemented by oxidative damage to the nanotube framework by strong acids which leave holes functionalized with oxygenated functional groups [18]. CNTs can also be functionalized covalently or non-covalently with various polymers. Covalent functionalization is usually performed by grafting methods [19–22]. The non-covalent approaches are based on interactions of the hydrophobic part of the adsorbed molecules with nanotubes sidewalls through van der Waals, π–π, CH–π, and other interactions, and aqueous solubility is provided by the hydrophilic part of the molecules. In the last few years, the non-covalent treatment of CNTs with surfactants and polymers has been widely used in the preparation of both aqueous and organic solutions to obtain high weight fraction of individually dispersed nanotubes [23–26].

Following our interest in the utilization of CNTs as a reinforcing filler for the preparation of polymer composites [27–31], herein we report the synthesis and characterization of *p*-aminophenol (p-AP) functionalized multi-walled CNT (MWCNT)/poly(amide-imide) (PAI) composites.

EXPERIMENTAL

Materials

A carboxyl-modified MWCNT (the outer-diameter 8–15 nm, the inner-diameter 3–5 nm, length ~50 μm, carboxyl content 2.56 wt %, and purity > 95 wt %), manufactured by a thermal chemical vapor deposition process, was purchased from Neutrino Co. (Iran). Other chemicals used in this study were obtained commercially from Fluka Chemical Co. (Switzerland), Aldrich Chemical Co. (Milwaukee, WI) and Merck Chemical Co. (Germany). *p*-Aminophenol, 3,5-dinitrobenzoylchloride, pyromellitic dianhydride (PMDA), *L*-phenylalanine (Phe) amino acid, glacial acetic acid, propylene oxide, tetrabutylammonium bromide (TBAB), and triphenyl phosphite (TPP) were used as received without further purification. Propylene oxide was used as acid scavenger. Hydrazine monohydrate and 10% palladium on activated carbon were used as received. DMF, and *N*,*N*'-dimethylacetamide (DMAc) as solvents were distilled over barium oxide under reduced pressure before use. Other reagents were used without further purification.

3,5-Diamino-*N*-(4-hydroxyphenyl)benzamide as a diamine monomer was prepared according to the reported procedure [32].

N,*N*'-(Pyromellitoyl)-bis-*L*-phenylalanine (7) was prepared according to our previous work and is shown in Scheme 1 [33].

Synthesis of PAI

According to Scheme 1, 0.10 g (1.95×10^{-4} mol) of diacid monomer **7**, 0.047 g (1.95×10^{-4} mol) of diamine **4**, and 0.25 g of TBAB (7.8×10^{-4} mol) were placed in a porcelain dish and ground completely for 5 min. Then, 0.2 mL (7.8×10^{-4} mol) of TPP was added and the mixture was ground for 3 min. The reaction mixture was irradiated in the microwave oven for 8 min at 50% of power level (900 W) (the temperature of the reaction was around 130°C). The resulting viscous solution was poured into 30 mL of methanol, filtered, and dried at 80°C for 6 h under vacuum to give 0.13 g (92%) of white powder PAI. The optical specific rotation was measured ($[\alpha]^{25}_{\text{Na, 589}} = -36.68$) at a concentration of 0.5 g/dL in DMF at 25°C. The inherent viscosity was also measured ($\eta_{\text{inh}} = 0.30$ dL/g) under the same conditions.

FTIR (KBr, cm^{-1}): 3370 (m, br, NH and OH stretching), 3114 (w, C–H aromatic), 2925 (w, C–H aliphatic), 1775 (m, C=O imide, asymmetric stretching), 1725 (s, C=O imide, symmetric stretching), 1601 (m, C=O amide, stretching), 1599 (s), 1575 (m), 1510 (s), 1445 (s), 1381 (m, CNC axial stretching), 1212 (m, CNC transverse stretching), 1104 (s), 832 (m), 726 (s, CNC out-of-plane bending), 649 (w). ^{1}H NMR (400 MHz, DMSO-d_6, ppm): 3.60–3.62 (dd, 4H, CH_2, distorted), 5.25 (dd, 2H, CH, distorted), 6.68–6.70 (d, 2H, Ar–H, $J = 6.32$ Hz), 7.03–7.05 (d, 2H, Ar-H, $J = 6.80$ Hz), 7.08–7.13 (m, 10H, Ar-H), 7.47 (s, 2H, Ar-H), 7.70 (s, 1H, Ar-H), 8.22 (s, 2H, Ar-H), 9.25 (s, 1H, OH), 10.08 (s, 2H, NH), 10.20 (s, 1H, NH). Elemental analysis: calculated for $(C_{30}H_{28}N_4O_7)_n$: C, 68.42%; H, 4.06%; N, 9.73%. Found: C, 66.75%; H, 4.81%; N, 9.49%.

Characterization

The equipment used for the functionalization of MWCNT and the fabrication of the polymer was a Samsung microwave oven (2450 MHz, 900 W) (Seoul, South Korea). Melting points of the monomers were measured on a melting-point apparatus (Gallenhamp,

Cambridge, United Kingdom) without correction. ^{1}H and ^{13}C NMR spectra were recorded on a Bruker (Rheinstetten, Germany) Avance 500 instrument at room temperature in DMSO-d_6. Multiplicities of proton resonance were designated as singlet (s), doublet (d), doublet of doublet (dd) and multiplet (m). ^{13}C NMR spectrum was broadband proton decoupled. FTIR spectra of the samples were recorded with a Jasco-680 (Tokyo, Japan) spectrometer [taken in potassium bromide (KBr)] at a resolution of 4 cm^{-1}. They were scanned at wavenumber range of 400–4000 cm^{-1}. Band intensities were assigned as weak (w), medium (m), strong (s), and broad (br). Vibration bands were reported as wavenumber (cm^{-1}). Elemental analysis was performed in an Elementar Analysensysteme GmbH (Hanau, Germany). Inherent viscosity was measured using a Cannon Fenske Routine Viscometer (Mainz, Germany) at the concentration of 0.5 g/dL in DMF and at 25°C. Optical specific rotation was measured at the concentration of 0.5 g/dL in DMF and at 25°C using a quartz cell (1.0 cm) with a Jasco Polarimeter (JASCO Co., Ltd., Tokyo, Japan). Thermal stability of MWCNTs, PAI and MWCNT-AP/PAI composites was evaluated by recording TGA traces (STA503 TGA, Bahr-Thermoanalyse GmbH, Hüllhorst, Germany) in nitrogen atmosphere (flow rate 60 cm^3/min). A heating rate of 10°C/min and a sample size of 10 ± 2 mg were used in each experiment. The XRD was used to characterize the crystalline structure of the samples. XRD patterns were collected using a Bruker, D8AVANCE (Rheinstetten, Germany) diffractometer with a copper target at the wave length of λ Cu$K_\alpha = 1.54$ Å, and a tube voltage of 40 kV, and tube current of 35 mA. The samples were scanned at a rate of 0.05°/min from 10° to 80° of 2θ. For XRD studies, rectangular pellets prepared by compression molding were used. The morphology of the MWCNTs and dispersion morphology of the MWCNTs-AP on the PAI matrix were observed using FE-SEM. The images were taken at 15 KV using a HITACHI S-4160 instrument (Tokyo, Japan). TEM images were obtained using a Philips CM 120 microscope (Germany) with an accelerating voltage of 100 kV. For TEM studies, ultra-thin sections (30–80 nm) of MWCNTs-AP and the composites were prepared using Leica Ultramicrotome. Tensile testing was performed at room temperature on a Testometric Universal Testing Machine M350/500 (Mainz, Germany), according to ASTM D 882 (standards). Tests were carried out with a cross-head speed of 12.5 mm/min until reaching a deformation of 20% and then, at a speed of 50 mm/min at break. The dimensions of the test specimens were $35 \times 2 \times 0.04$ mm. Property values reported here represented an average of the results for tests run on at least five specimens. Tensile strength, tensile modulus, and strain were obtained from these measurements. Preparation of MWCNT-AP/PAI composites was carried out on a MISONIX ultrasonic XL-2000 SERIES (Raleigh, North Carolina, USA). Ultrasonic irradiation was performed with the probe of the ultrasonic horn being immersed directly in to the mixture solution system with the frequency of 2.25×10^4 Hz and the power of 100 W.

Functionalization of MWCNTs and Fabrication of the MWCNT-AP/PAI Composites

The functionalization procedure was based directly on our previously reported pathway, which was able to attach MWCNTs benzene rings with amino functional groups [34].

3 mL of DMAc and the appropriate amount (from 5 to 15 wt %) of MWCNTs-AP were placed in a beaker and stirred for 24 h at 30–40°C to reach a homogenous suspension (beaker A). About 1 g of PAI and 1.5 mL DMAc were placed in another beaker and stirred 24 h at room temperature (beaker B). Next, the solutions of beakers A and B were combined and stirred for 24 h, followed by ultrasonication for 1 h. The nanocomposite films were prepared by coating 3 mL of the final mixture solution on a piece of glass slide. The resultant films were dried in an oven. The casting process was completed in a heating program shown as follow: ramping from room temperature to 60°C in 30 min, keeping at 60°C for 24 h, then ramping from 60 to 160°C in 8 h, keeping at 160°C for 45 min, and finally cooling to room temperature.

RESULTS AND DISCUSSION

Monomer and Polymer Synthesis and Characterization

Diacid monomer **7** was synthesized by the condensation reaction of an equimolar amount of PMDA and *L*-phenylalanine in reflux acetic acid solution (Scheme 1) [33]. Diamine monomer **4** was synthesized using a two-step process (Scheme 1). In the first step, aromatic nucleophilic displacement of 3,5-dinitrobenzoylchloride with p-AP in the presence of propylene oxide in DMAc solvent resulted in *N*-(4-hydroxyphenyl)-3,5-dinitrobenzamide (3) as a pale yellow solid. In the second step, this dinitro was reduced in ethanol in the presence of hydrazine hydrate and a catalytic amount of palladium on the activated carbon at 80°C, producing yellow crystals of the diamine 4. The structure of the dinitro 3 and diamine 4 was identified by elemental analysis, FTIR, ^{1}H NMR, and ^{13}C NMR spectroscopy [32].

A good number of methods for the synthesis of PAIs have been reported. Some of them require a prolonged reaction time and the use of toxic solvents. The growing interest during the last two decades in the environmental protection has made both modern academic and industrial groups develop green chemical processes with maximum yield and minimum cost [35–37]. As a part of our program, we aimed at the development of synthetic methodologies [38, 39] by eliminating flammable, toxic, or carcinogenic organic solvents and employed a molten ionic salt, TBAB, as a

green chemical medium for step-growth polymerization. The rapid use of microwave activation as a nonconventional energy source in organic chemistry also helped us in devising the above synthetic route. A synthetic strategy, using molten TBAB and microwave irradiation collectively, was found to be a successful and efficient method for the synthesis of polymers [40]. Consequently, the mixture of monomers **4** and **7** was irradiated under microwave (optimized condition; 50% of power level, 130°C) with TBAB in the presence of TPP for 8 min. We observed that the PAI was obtained in 92% of isolated yield. Thus, we found that molten TBAB salt was a highly polar medium that was likely to be strong microwave absorption. The inherent viscosity of the synthesized PAI was 0.32 dL/g. The resulting polymer showed optical rotation, indicating that the polymer was optically active and chirality was introduced into the backbone of the polymer. The optical specific rotation of this polymer was $[\alpha]^{25}_{Na,\,589} = -42.18$ (0.05 g in 10 mL of DMF). The structure of this polymer was confirmed by FTIR spectroscopy, ^{1}H NMR, and elemental analysis techniques [41]. The solubility of this polymer was investigated with 0.01 g polymeric sample in 2 mL of solvent. The obtained polymer can be dissolved in organic solvents such as DMF, DMAc, DMSO and *N*-methyl-2-pyrrolidone (NMP) at room temperature and it was insoluble in solvents such as chloroform, methylene chloride, methanol, ethanol and water.

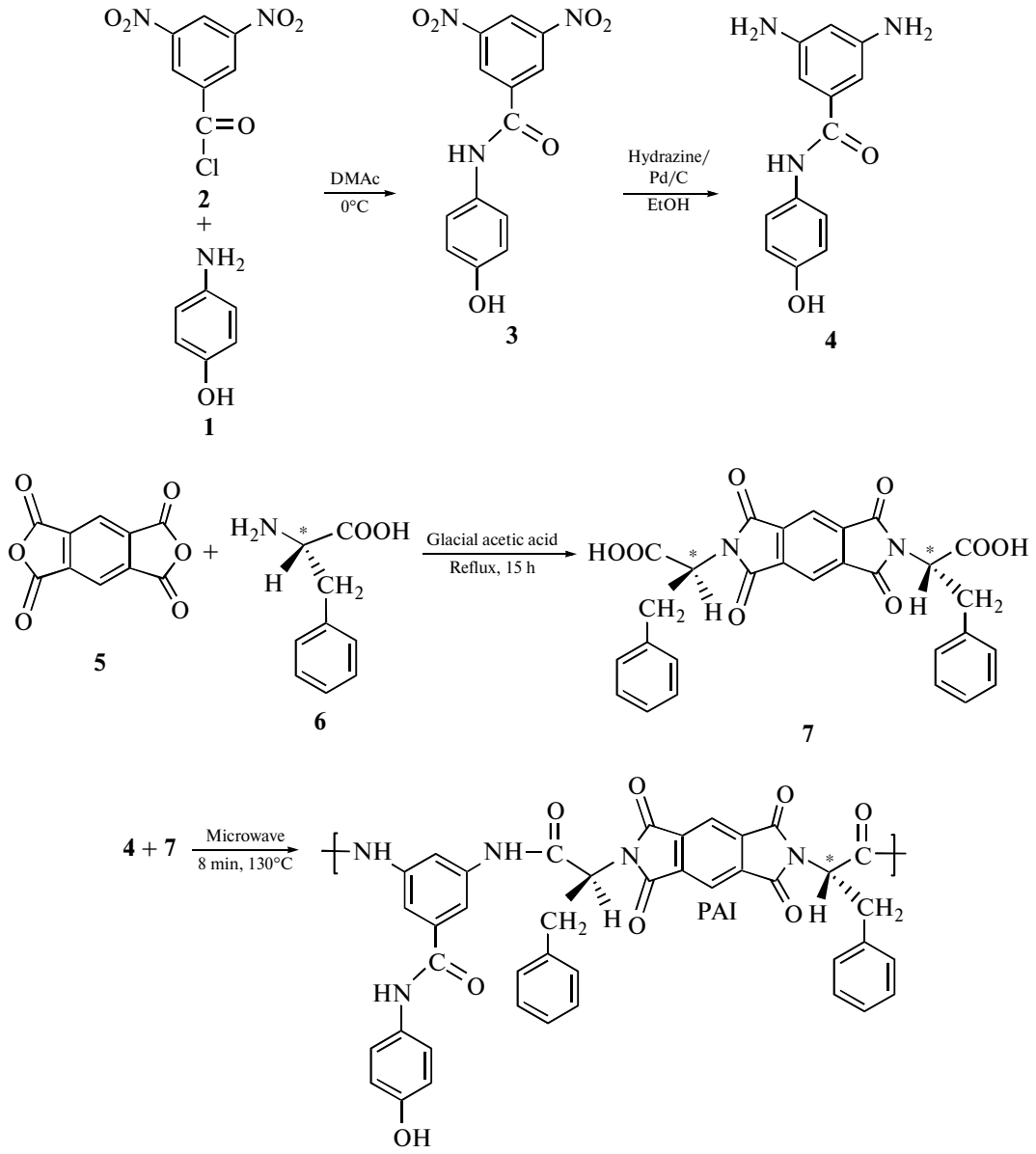

Scheme 1. Synthetic outline for the preparation of PAI.

Preparation of MWCNTs-AP and MWCNT-AP/PAI Hybrid Films

Scheme 2 shows the schematic diagram of functionalization procedure of MWCNTs with p-AP, which is inexpensive and an available reagent [34]. Functionalization was carried out under microwave irradiation according to a previous work [42]. Surface functionality groups and the morphology of MWCNTs were analyzed by FTIR spectroscopy, XRD, TGA, FE-SEM, and TEM.

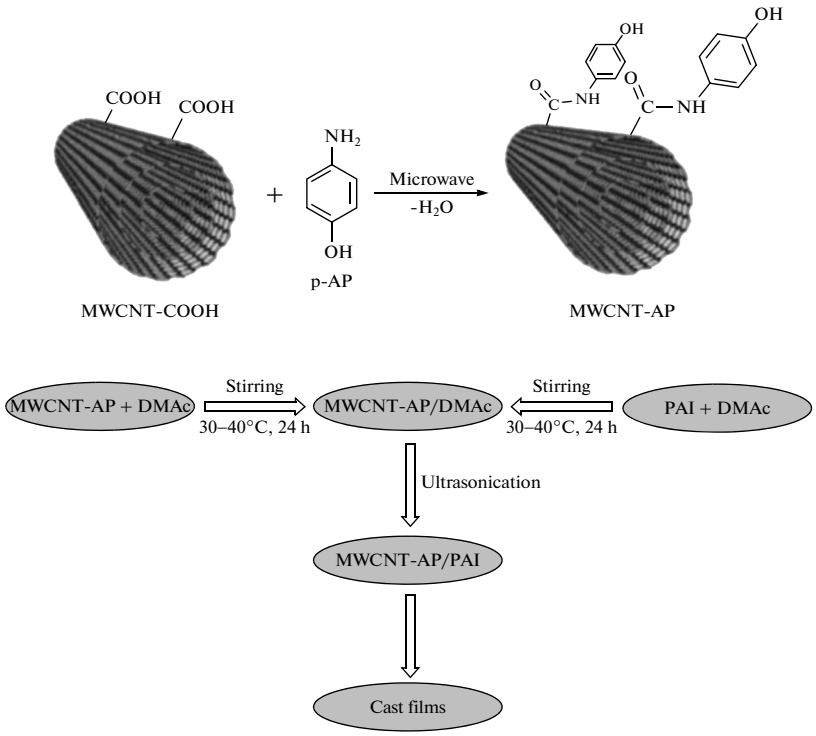

Scheme 2. Schematic of the preparation process of MWCNT-AP and MWCNT-AP/PAI composites.

The dispersion of the MWCNTs-AP in 5, 10, and 15 wt % solutions of PAI in DMAc was achieved by vigorous stirring with a speed of 15000 rpm for 1 day, using a homogenizer, which was followed by utrasonication process for 1 h to form a new series of chiral composites. The reaction pathway for preparing MWCNT-AP/PAI composites is shown in Scheme 2. The effective use of CNTs in composite applications depends on the ability to disperse the CNTs uniformly throughout the matrix without reducing their aspect ratio. Due to the van der Waals attraction, CNTs are held together as bundles and ropes. Therefore, they have a very low solubility in solvents and tend to remain as entangled agglomerates. To employ CNTs as an effective reinforcement in polymer composites and ensure proper dispersion and appropriate interfacial adhesion between the CNTs and polymer matrix, several mechanical/physical methods were used [5–9]. So, in this study, at first, the MWCNTs were functionalized with p-AP. In our previous studies about the production of CNT/polymer composites, we used 5–15 wt % of MWCNT loading and good results were found [27–31]. Several researches have also investigated the properties of CNT/polymer composites with CNT content from 1–15 wt % and good results have been reported [43–45]. So, in this study, we selected 5–15% of CNT content in the composites. The introduction of a number of functional groups into the backbone of aromatic polymer performs a hydrogen bonding with modified CNTs and a composite based on hydrogen bond by which PAI chains are tightly attached to the surface of MWCNT-AP, as can be seen schematically in Fig. 1.

Characterization of Materials

FTIR spectra (Fig. 2) can serve a qualitative characteristic of AP-functionalized nanotubes. In contrast to acid-functionalized MWCNTs, the MWCNT-AP samples provided good evidence for the desired functionalities. The spectrum of a carboxylated MWCNTs/KBr pellet showed a strong, broad absorption band centered at 3433 cm^{-1}, which could be attributed to the O–H stretching bands of carboxylic acid moieties from the surface of MWCNTs. The band around 2923 cm^{-1} was ascribed to aliphatic sp^3 C–H of MWCNTs [46]. Strong band of absorption characteristic for the acid linkage appeared at 1629 cm^{-1} assigned to C=O stretching vibration. The N–H groups that were observed on the functionalized sam-

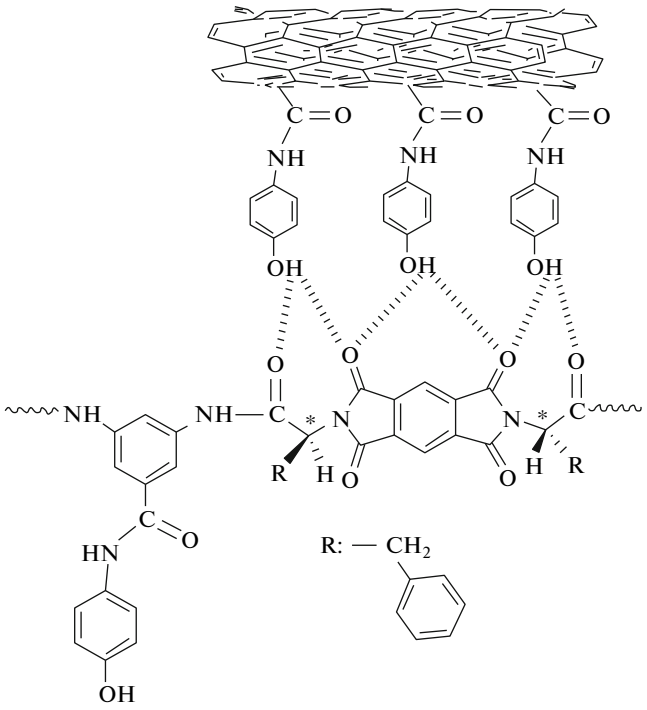

Fig. 1. Possible H-bonds between functional groups along a functionalized nanotube and the PAI chains.

ples and the appeared band at 1384 cm^{-1}, which is attributed to the C–N–C axial stretching bands could indicate that the amidation reactions occurred between the amino group of p-AP and the carboxyl groups on the surfaces of the MWCNTs. The intensities of the bands at 3399 cm^{-1} and at around 1625 cm^{-1}, which were assigned to the stretching vibration of O–H bond and C=O of amide bond, respectively, indicated that the p-AP had been successfully attached to the surface of MWCNTs.

The formation of PAI was also confirmed by using FTIR spectroscopy. Strong absorption bands were observed at 1775 cm^{-1}. This can be attributed to the asymmetric and symmetric stretching vibrations of the imide carbonyl groups. The bands of C–N bond stretching and ring deformation appeared at 1381 and 726 cm^{-1}. Strong bands of absorption were characteristic of the hydroxyl group and the newly formed amide linkage appeared at around 3370 cm^{-1}. They were assigned to O–H and N–H stretching vibrations at 1601 cm^{-1}, which can be attributed to amide C=O stretching vibration; and at 1575 cm^{-1}, they were due to N–H bending vibration. The absorption band at around 3114 cm^{-1} was attributed to =CH aromatic linkage. The aliphatic C–H stretching peak was also appeared at around 2925 cm^{-1} [47]. The presence of CNTs in the polymer matrix showed very few changes in the FTIR spectrum, presumably due to the low MWCNT composition and the weak vibration signals of MWCNTs. Figure 2 shows the FTIR spectra of MWCNT-AP/PAI composites.

The structure of neat PAI was also identified by ^1H NMR spectroscopy. In the ^1H NMR spectrum of this polymer (Fig. 3), appearances of the N–H protons of amide groups and O–H group at 10.08, 10.20, and 9.25 ppm as three singlet peaks, respectively, indicate the presence of amide groups in the polymer's side chain as well as main chain and hydroxyl group in the polymer's side chain. The resonance of aromatic protons appeared in the range of 6.68–8.22 ppm. The proton of the chiral center appeared as doublet at 5.25 ppm.

The XRD patterns of the samples are shown in Fig. 4. The X-ray patterns of the MWCNT displayed the presence of two peaks at $2\theta = 26°$ and 44° corresponding to the (0 0 2) diffraction plane of the impurity graphite, and α-Fe (1 1 0) and/or Ni (1 1 1) reflections [48]. MWCNTs-AP showed very few changes in the XRD pattern. It could be seen that XRD pattern is very similar to the carboxylated MWCNTs. Pure PAI showed broad diffraction peaks at $2\theta = 20°$. The X-ray patterns of the MWCNT/PAI composites showed mixed peaks appearing in the MWCNT-AP and pure PAI, respectively. The intensity of the peaks assigned to the MWCNT-AP in the composites increased with the increase of MWCNTs-AP content.

Figure 5 presents FE-SEM images of the pristine MWCNTs-COOH and MWCNTs-AP. The FE-SEM image of the MWCNTs-COOH surface is about flat. After functionalization with p-AP, the surface of MWCNTs became an irregular debundled structure, as can be seen in Fig. 5. FE-SEM images of fracture surfaces of neat PAI and composites were also observed to characterize the morphology and dispersity of MWCNTs-AP in the composites, as displayed in Fig. 6. The neat PAI copolymer showed a spongy morphology. FE-SEM observation revealed that the PAI particles were self-organized into nanopatterns. As shown, the average diameter of polymeric particles was about 68 nm. The homogeneous dispersion of MWCNTs-AP in the PAI matrix may be due to the fact that induced hydrogen bonding and van der Waals force between polymer and CNTs during formation of composite films. For all composites, the FE-SEM images showed that MWCNTs-AP are homogeneously dispersed in the polymer matrix.

Figure 7 shows TEM images of the MWCNT-COOH (bottom) and MWCNT-AP (up). As can be seen, they depict a high surface roughness for the MWCNTs-AP. This surface roughness may imply the partial damage of graphitic carbon, which could have resulted from the severe functionalization and/or oxidation processes [49]. Although TEM could not distinguish minute functional groups, it could represent surface deterioration of the CNTs that occurred as a result of functionalization. As mentioned above, the functionalization reaction disrupted the sp^2 carbon network of graphitic CNTs, so it may be responsible for the roughness of CNTs' surfaces. In fact, since the microwave radiation was harsh enough to produce

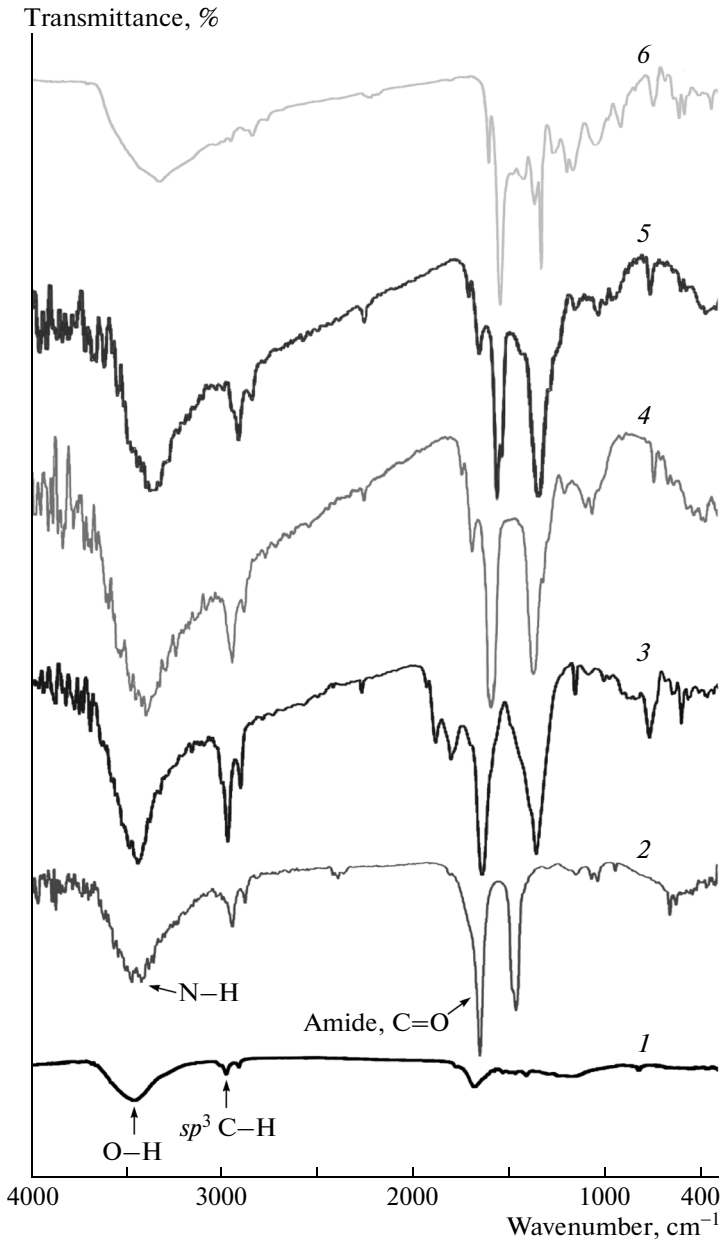

Fig. 2. FTIR spectra of MWCNT-COOH and MWCNT-AP, PAI, and the MWCNT-AP/PAI composites: (*1*) MWCNT-COOH, (*2*) MWCNT-AP, (*3*) CNT-AP/PAI 15%, (*4*) CNT-AP/PAI 10%, (*5*) CNT-AP/PAI 5%, (*6*) neat PAI.

highly disordered carbon (Fig. 7), it is likely that it could also damage graphitic MWCNTs [50]. The representative TEM images of the MWCNT/PAI composites are shown in Fig. 8. In general, the drawbacks related to the homogeneous dispersion of the CNTs in the polymer matrix resulted from the intrinsic van der Waals attractions between the individual CNTs in combination with high aspect ratio and large surface area. This made it difficult for the CNTs to disperse in the polymer matrix. The interfacial adhesion between the CNTs and the polymer matrix plays an important role in improving the properties of the polymer composites. As shown in Fig. 8, the MWCNTs-AP were dispersed well in the composites. This can be explained by the fact that the MWCNT stabilizes their dispersion by good interactions with the PAI matrix, resulting from the increased polarity by the functional groups formed on the surfaces of the MWCNTs as well as good interactions of the carboxyl groups with the carbonyl groups of the PAI matrix. The presence of the functional groups on the surfaces of the MWCNTs resulted in the interfacial interaction between the polymer matrix and the CNTs in the composites. For example, a hydrogen bonding could be formed between the carbonyl groups at the MWCNT-AP with

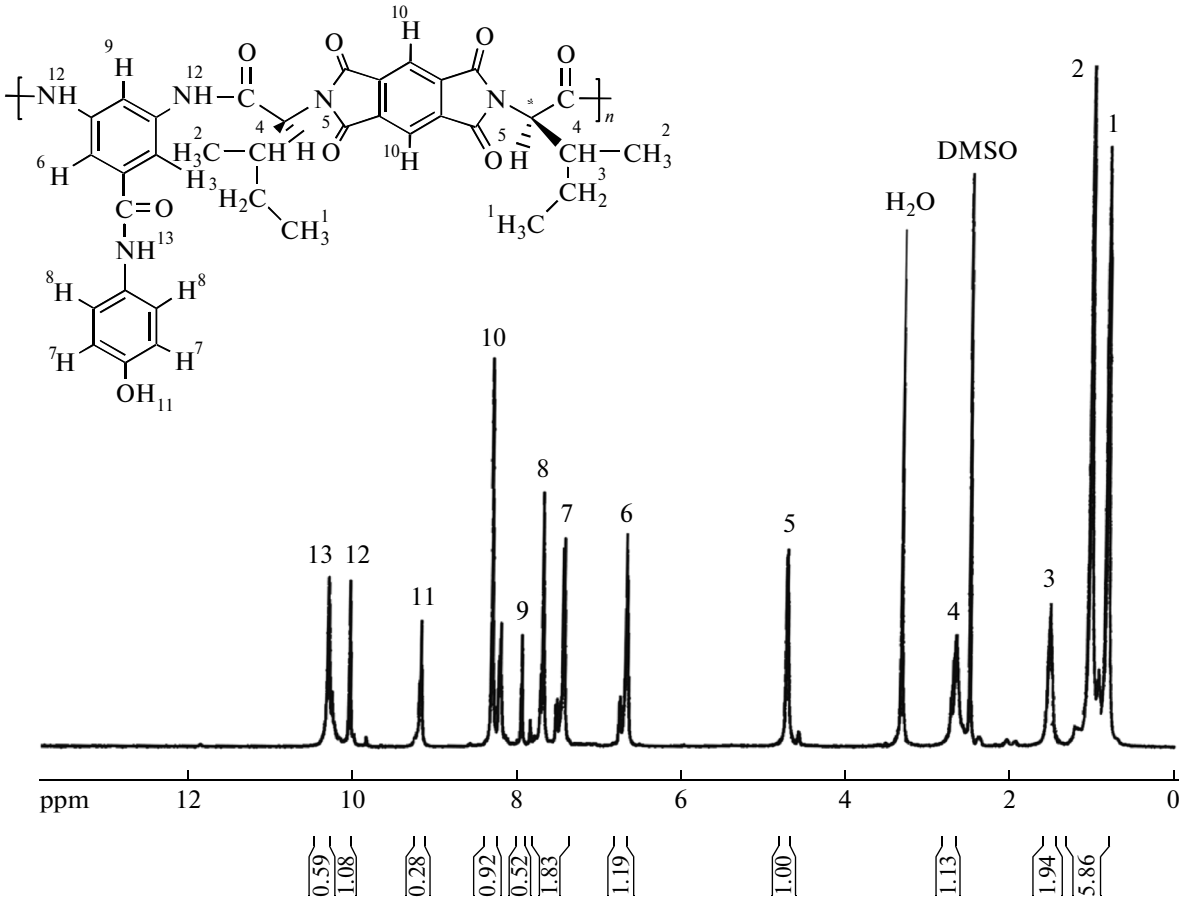

Fig. 3. ^{1}H NMR (400 MHz) spectrum of PAI.

the oxygen atoms at the carbonyl groups of PAI chains (Fig. 1).

Figure 9 shows the TGA thermograms of the samples as measured in nitrogen atmosphere. It is observed that the mass loss takes place in a single-step mechanism. Besides, the results obtained from these analyses are completely given in Tables 1 and 2. The thermogram of pristine CNT showed a small mass loss in a temperature range of 0–550°C. The weight loss of MWCNT-AP resulted from the decomposition of the functionalized organic moieties attached to the surface of MWCNTs. TGA data of the pristine and the purified MWCNTs suggested that the MWCNTs were able to withstand oxidation temperatures up to 700°C. This could be due to the incorporation of –COOH groups in the defective sites and tips. The TGA plot showed that the degradation of specimen MWCNT-AP occurred in the 240–700°C temperature range. By comparing the MWCNTs-AP with MWCNTs-COOH, it can be concluded that the thermal stability of MWCNTs-COOH was destroyed upon functionalization with p-AP. The thermal behavior data for the PAI and the composites are summarized in Table 2. The onset of decomposition temperature of the composites was higher than that of pure PAI, shifting toward higher temperatures as the amount of MWCNT was increased. The marginal increase in thermal stability of PAI matrix upon incorporation of MWCNTs-AP could be attributed to the higher thermal conductivity of CNTs that facilitated heat dissipation within the composites, hence preventing the accumulation of heat at certain points for degradation [51]. The end temperature of decomposition was also retarded with increasing MWCNT-AP content. The weight percent remaining after major degradation at 800°C was higher for composites rather than neat PAI. This indicated that MWCNT-AP reduced the degradation of PAI at high temperature. So, it could be con-

Table 1. Thermal stability of CNT samples obtained from TGA thermograms[a]

Sample	T_5, °C	Weight residue at 800°C
MWCNT-COOH	550	90
MWCNT-AP	325	73

[a] Temperature at which 5% weight loss was recorded by TGA at a heating rate of 10°C min^{-1} in a nitrogen atmosphere.

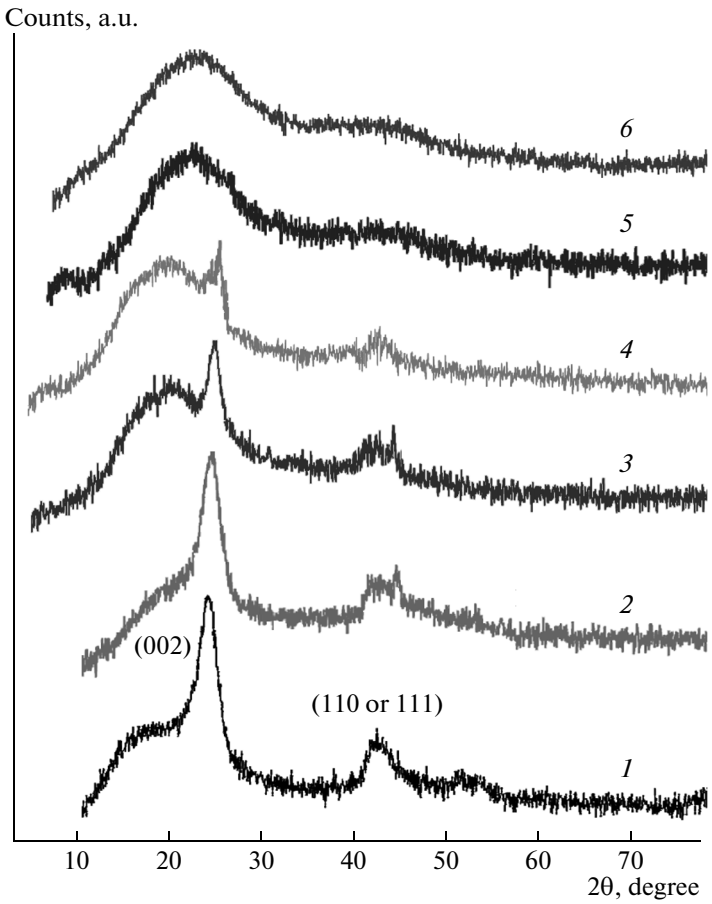

Fig. 4. XRD pattern for MWCNT-COOH, MWCNT-AP, and MWCNT-AP/PAI composite samples with different MWCNT-AP contents: (*1*) MWCNT-COOH, (*2*) MWCNT-AP, (*3*) CNT-AP/PAI 15 wt %, (*4*) CNT-AP/PAI 10 wt %, (*5*) CNT-AP/PAI 5 wt %, (*6*) neat PAI.

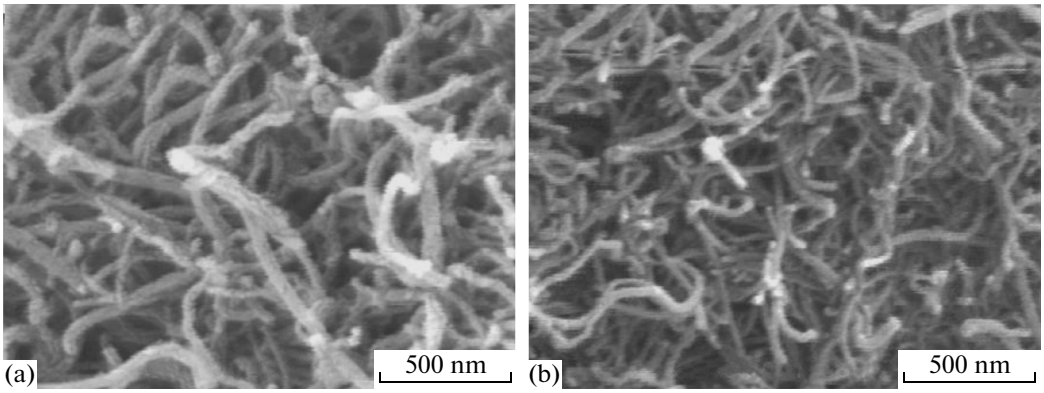

Fig. 5. FE-SEM images of (a) MWCNT-COOH and (b) MWCNT-AP.

firmed that a small amount of MWCNT acted as effective thermal degradation resistant reinforcement in the PAI matrix, increasing the thermal stability of the MWCNT/PAI composites.

The limiting oxygen index (LOI) is the minimum concentration of oxygen, expressed as a percentage, which will support combustion of a polymer. It can be used to evaluate the flame retardancy of the polymers. Normal atmospheric air is approximately 21% oxygen, so a material with an LOI of less than 21% would burn easily in air. That being said, a material with LOI of greater than 21% but less than 28% would be consid-

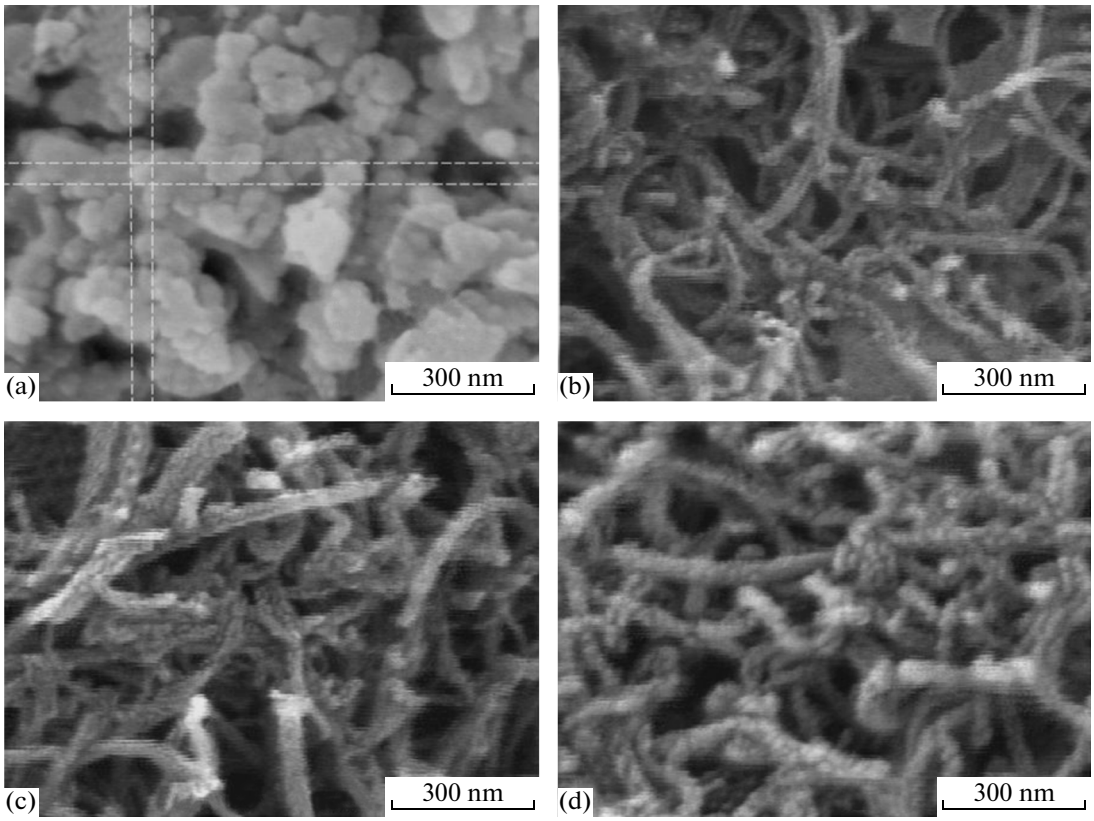

Fig. 6. FE-SEM images of a fracture surface of the produced materials: (a) pristine PAI and composites containing (b) 5 wt %, (c) 10 wt %, and (d) 15 wt % MWCNTs-AP.

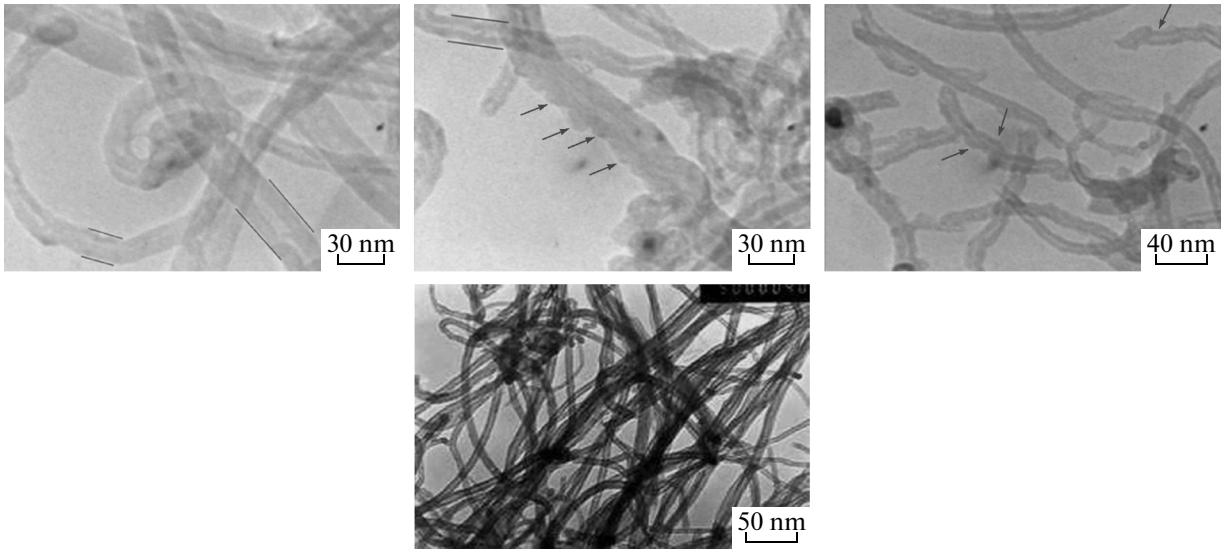

Fig. 7. TEM images of MWCNT-AP (top) and MWCNT-COOH (bottom) at two different magnifications.

ered "slow burning". A material with LOI of greater than 28% would be considered "self-extinguishing". A self-extinguishing material is one that would stop burning after the removal of the fire or ignition source. Theoretically, two interesting relationships have been found between the LOI and the parameters of the combustion process: char yield or char residue (CR) and heat of combustion. According to the equation given below (Eq. 1), there is a linear relationship between LOI and CR only for halogen-free polymers [52]:

$$\mathrm{LOI} = (17.5 + 0.4CR)/100 \quad (1)$$

From this equation, a higher char yield will improve flame retardancy. PAI and composites, containing 5, 10, and 15 wt %, had LOI values of 35.1, 36.3, 37.5, and 39.1, respectively, as calculated from their CR. On the basis of the LOI values, such materials can be classified as self-extinguishing materials. Furthermore, according to the another equation given below (Eq. (2)), the LOI values of many general materials can be reasonably well predicted by the equation [53]:

$$\mathrm{LOI} = 8000/\Delta H_{comb}, \quad (2)$$

where ΔH_{comb} is the specific heat of combustion in J/g. As a result, PAI and composites, containing 5, 10, and 15 wt %, had ΔH_{comb} values of 22.8, 22.0, 21.3, and 20.5 kJ/g, respectively.

MWCNTs-AP were also found to greatly enhance the mechanical properties of PAI due to the nanoreinforcing effect of CNT with high aspect ratio. The mechanical tensile properties of PAI hybrid films with various MWCNT-AP contents are shown in Fig. 10. It can be seen that, in comparison with neat PAI film, the MWCNT-AP/PAI composite films exhibit higher Young's modulus and tensile strength but smaller strain at break, and the strain at break decreases gradually with increasing MWCNT-AP feeding content, while a significant increment in Young's modulus and a moderate increment in tensile strength are observed simultaneously. As shown in Fig. 10, the Young's mod-

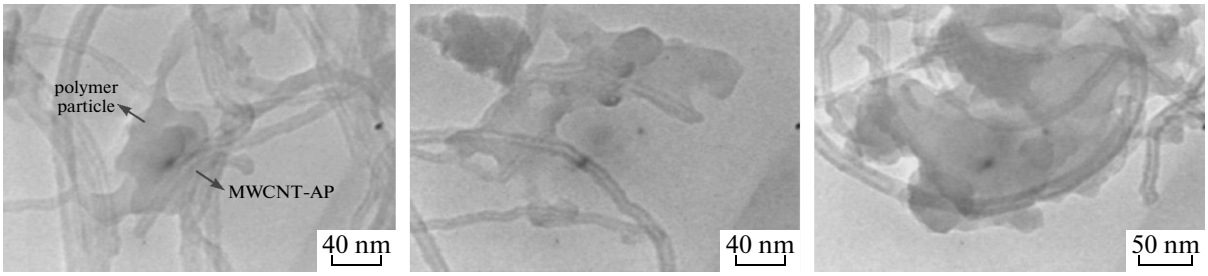

Fig. 8. TEM micrographs of MWCNTs-AP dispersed in composites containing 10 wt % of MWCNTs-AP.

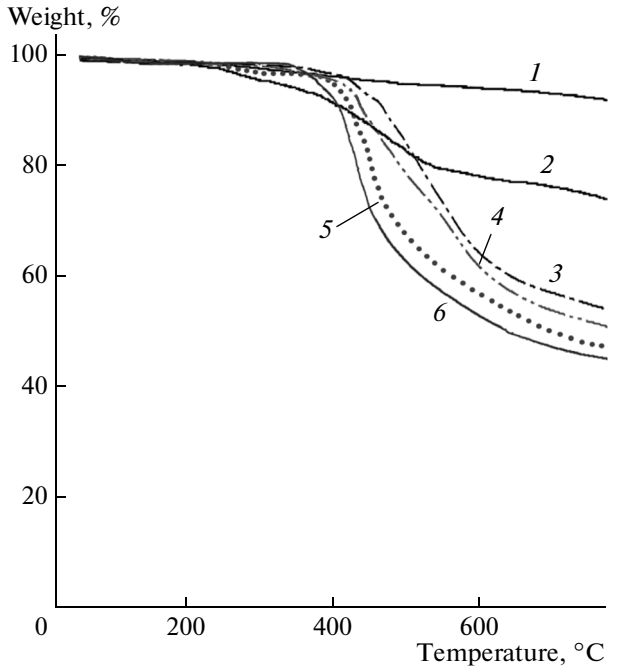

Fig. 9. TGA results of carboxylated (*1*) and *p*-aminophenol (*2*) functionalized MWCNTs, composites containing 5–15 wt % of MWCNTs-AP (*3*–*5*), and neat PAI (6).

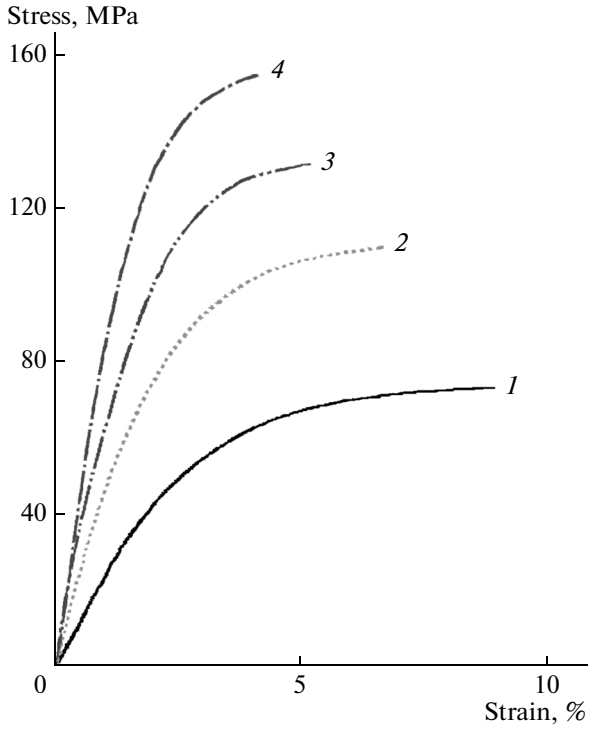

Fig. 10. Tensile stress-strain curves of MWCNTs-AP/PAI composites for concentrations ranging from 0 to 15% MWCNTs-AP by weight: (*1*) neat PAI, (*2*) CNT/PAI 5 wt %, (*3*) CNT/PAI 10 wt %, (*4*) CNT/PAI 15 wt %.

Table 2. Thermal properties of PAI and the composites[a]

MWCNTs-AP content, %	T_5^a, °C	T_{10}^a, °C	CR[b], %	LOI, %[c]	ΔH_{comb}, kJ/g
0	394	408	44	35.1	22.8
5	400	431	47	36.3	22.0
10	417	448	50	37.5	21.3
15	438	477	54	39.1	20.5

[a] Temperature at which 5 and 10% weight loss was recorded by TGA at a heating rate of 10°C min^{-1} in a nitrogen atmosphere.
[b] Percentage weight of material left undecomposed after TGA analysis at maximum temperature 800°C in a nitrogen atmosphere.
[c] Limiting oxygen index (LOI) evaluating at char yield at 800°C.

ulus and tensile strength increase from 1.8 ± 0.1 GPa and 78.3 ± 1.2 MPa for neat PAI film to 3.1 ± 0.2 GPa and 114.3 ± 1.1 MPa, 3.4 ± 0.2 GPa and 132.5 ± 1.1 MPa, and 3.7 ± 0.1 GPa and 155.1 ± 0.9 MPa for MWCNT-AP/PAI composite film with increasing the MWCNT-AP feeding content from 5 to 10 and 15 wt %, respectively. The value in 112.4 MPa for the sample with 5 wt % MWCNTs loading was 46.0% higher than that of the pure PAI. Compared to previous study in the use of carboxylated MWCNTs [31, 40], this improvement was not observed. By using unfunctionalized CNTs, incorporation of 5% MWCNTs into the PAI film increased its tensile strength to 60.4 MPa, which is about 39.6% higher than that of the pure PAI counterpart. The reinforcing efficiency of MWCNT-AP is defined as the normalized mechanical properties of the composites with respect to those of pure PAI. The general tendency for improvement in the stress level is increased by the addition of CNTs which play the role of reinforcement. Another reason for the enhancements in the tensile modulus of composites is the strong interaction between the PAI matrix and MWCNTs-AP via formation of hydrogen and non-covalent bonding.

CONCLUSIONS

In conclusion, we reported on the covalent functionalization of MWCNTs with an electron-withdrawing substituent, p-AP, in a simple, low cost, and efficient method involving the use of microwave technology, as a means of improving the state of dispersion of MWCNTs in the polymer matrix. The occurrence of p-AP functionalization of the nanotubes was confirmed by the use of several methods usually used in materials science. The attached p-AP groups were expected to improve the interaction between the MWCNTs-AP and polymer molecule chains. The terminal hydrophilic hydroxyl groups of phenol moieties are able to undergo additional reactions such as covalent binding with a variety of monomer and polymer matrices in the processing and fabrication of composites and fibers. Modification with p-AP resulted in a significant debundling of the MWCNTs, allowing stable dispersion in common polar organic solvents. Compared to other CNT/polymer nanocomposites, in this study, it was observed that by the incorporating of MWCNT-AP, better results were obtained in the case of thermal and mechanical properties [54, 55]. The successful fabrication of high-quality composites shows that the MWCNT functionalization with p-AP improves the solubility and processing of nanotubes, enabling their incorporation into polymer composite materials through non-covalent bonding to the surrounding matrix via terminal functional groups on nanotubes. Functionalization with p-AP molecule by microwave radiation seems to provide the best interaction with PAI matrix, leading to the highest value of composite properties.

ACKNOWLEDGMENTS

This study was supported by the Research Affairs Division of Isfahan University of Technology (IUT), National Elite Foundation (NEF), and Center of Excellency in Sensors and Green Chemistry Research (IUT).

REFERENCES

1. D.-S. Bang, K. H. Yoon, Y.-B. Park, D.-Y. Lee, and S.-S. Jeong, J. Compos. Mater. **44**, 2711 (2010).
2. L. Hu, D. S. Hecht, and G. Gruner, Chem. Rev. **110**, 5790 (2010).
3. N. G. Sahoo, S. Rana, J. W. Cho, L. Li, and S. H. Chan, Prog. Polym. Sci. **35**, 837 (2010).
4. S. R. Shin, S. M. Jung, M. Zalabany, K. Kim, P. Zorlutuna, S. B. Kim, M. Nikkhah, M. Khabiry, M. Azize, and J. Kong, ACS Nano **7**, 2369 (2013).
5. L. Li, W. Feng, and K. Pan, Colloids Surf., B **102**, 124 (2013).
6. M. Khaneft, B. Stuhn, J. Engstler, H. Tempel, J. J. Schneider, T. Pirzer, and T. Hugel, J. Appl. Phys. **113**, 074305 (2013).
7. L. D. Tijing, C.-H. Park, W. L. Choi, M. T. G. Ruelo, A. Amarjargal, H. R. Pant, I.-T. Im, and C. S. Kim, Composites, Part B **44**, 613 (2013).
8. N. K. Naik, K. S. Pandya, V. R. Kavala, W. Zhang, and N. A. Koratkar, J. Compos. Mater. **49**, 903 (2015).
9. G. Bayley, M. Hedenqvist, and P. Mallon, Polymer **52**, 4061 (2011).
10. C. Yu-Hsun, W. Ming-Sung, and L. King-Fu, J. Polym. Res. **21**, 1 (2014).
11. J. Cveticanin, A. Krkljes, Z. Kacarevic-Popovic, M. Mitric, Z. Rakocevic, D. Trpkov, and O. Neskovic, Appl. Surf. Sci. **256**, 7048 (2010).
12. J. Wang, M. Miao, Z. Wang, W. Humphries, and Q. Gu, Carbon **57**, 217 (2013).
13. Y. Wu, Z. Guo, and Y. Feng, Colloid Polym. Sci. **292**, 281 (2014).

14. S. Sagar, N. Iqbal, A. Maqsood, M. Shahid, N. A. Shah, T. Jamil, and M. I. Bassyouni,. J. Compos. Mater. **49**, 995 (2015).
15. M. K. Kim, K. Shanmuga Sundaram, G. Anantha Iyengar, and K.-P. Lee, Chem. Eng. J. **267**, 51 (2015).
16. H. Chen, S. Zeng, M. Chen, Y. Zhang, and Q. Li, Carbon **92**, 271 (2015).
17. B. Yu, Z. Liu, C. Ma, J. Sun, W. Liu, and F. Zhou, Tribol. Int. **81**, 38 (2015).
18. D.-J. Yun, and S.-W. Rhee, ACS Appl. Mater. Interfaces **4**, 982 (2012).
19. T. Morishita, M. Matsushita, Y. Katagiri, and K. Fukumori, Carbon **47**, 2716 (2009).
20. Y. Yang, C. P. Tsui, C. Y. Tang, S. Qiu, Q. Zhao, X. Cheng, Z. Sun, R. K. Y. Li, and X. Xie, Eur. Polym. J. **46**, 145 (2010).
21. R. M. Novais, J. A. Covas, and M. C. Paiva, Composites, Part A **43**, 833 (2012).
22. T. Macdonald, C. T. Gibson, K. Constantopoulos, J. G. Shapter, and A. V. Ellis, Appl. Surf. Sci. **258**, 2836 (2012).
23. T. Morishita, M. Matsushita, Y. Katagiri, and K. Fukumori, Carbon **48**, 2308 (2010).
24. S. C. Chou and Y. Y. Cheng, Polym. Polym. Compos. **20**, 353 (2012).
25. P. Ma and J. T. Spencer, J. Mater. Sci. **50**, 313 (2015).
26. M. Assali, M. P. Leal, I. Fernández, P. Romero-Gomez, R. Baati, and N. Khiar, Nano Res. **3**, 764 (2010).
27. S. Mallakpour and A. Zadehnazari, Polymer **54**, 6329 (2013).
28. S. Mallakpour and A. Zadehnazari, J. Solid State Chem. **211**, 136 (2014).
29. S. Mallakpour and A. Zadehnazari, J. Polym. Res. **20**, 1 (2013).
30. S. Mallakpour and A. Zadehnazari, Polym. Bull. **71**, 2523 (2014).
31. S. Mallakpour and A. Zadehnazari, Colloid Polym. Sci. **291**, 1525 (2013).
32. I. In and S. Y. Kim, Macromol. Chem. Phys. **206**, 1862 (2005).
33. S. E. Mallakpour, A. R. Hajipour, and S. Habibi, J. Appl. Polym. Sci. **86**, 2211 (2002).
34. S. Mallakpour and A. Zadehnazari, Polym. Int. **54**, 1203 (2014).
35. J. Pang, Y. Luan, Q. Wang, J. Du, X. Cai, and Z. Li, Colloids Surf., A **360**, 6 (2010).
36. R. Shahid, M. Gorlov, R. El-Sayed, M. S. Toprak, A. Sugunan, L. Kloo, and M. Muhammed, Mater. Lett. **89**, 316 (2012).
37. B. Liu, Z. Zhang, and Z. K. Zhao, Chem. Eng. J. **215–216**, 517 (2013).
38. S. Mallakpour and A. Zadehnazari, Polym. Plast. Technol. Eng. **51**, 1090 (2012).
39. S. Mallakpour and A. Zadehnazari, High Perform. Polym. **22**, 567 (2010).
40. S. Mallakpour and A. Zadehnazari, Soft Mater. **11**, 494 (2012).
41. S. Mallakpour and A. Zadehnazari, Polym. Sci., Ser. B **54**, 314 (2012).
42. H.Z. Zardini, A. Amiri, M. Shanbedi, M. Maghrebi, and M. Baniadam, Colloids Surf., B **92**, 196 (2012).
43. M. H. Al-Saleh and U. Sundararaj, Carbon **47**, 1738 (2009).
44. K. Bui, B. P. Grady, and D. V. Papavassiliou, Chem. Phys. Lett. **508**, 248 (2011).
45. F. Peng, F. Pan, H. Sun, L. Lu, and Z. Jiang, J. Membr. Sci. **300**, 13 (2007).
46. H.-J. Lee, S.-J. Oh, J.-Y. Choi, J. W. Kim, J. Han, L.-S. Tan, and J.-B. Baek, Chem. Mater. **17**, 5057 (2005).
47. S.-H. Hsiao, W. Guo, W.-F. Lee, Y.-C. Kung, and Y.-J. Lee, Mater. Chem. Phys. **130**, 1086 (2011).
48. M. Perez-Cabero, I. Rodrıguez-Ramos, and A. Guerrero-Ruız, J. Catal. **215**, 305 (2003).
49. A. Amiri, M. Maghrebi, M. Baniadam, and S. Zeinali Heris, Appl. Surf. Sci. **257**, 10261 (2011).
50. E. Vázquez and M. Prato, ACS Nano **3**, 3819 (2009).
51. S. T. Huxtable, D. G. Cahill, S. Shenogin, L. Xue, R. Ozisik, P. Barone, M. Usrey, M. S. Strano, G. Siddons, and M. Shim, Nat. Mater. **2**, 731 (2003).
52. D. Van Krevelen, Polymer **16**, 615 (1975).
53. P. Johnson, J. Appl. Polym. Sci. **18**, 491 (1974).
54. S. H. Lee, S. H. Choi, J. I. Choi, J. R. Lee, and J. R. Youn, Korean J. Chem. Eng. **27**, 658 (2010).
55. S. H. Lee, S. H. Choi, S. Y. Kim, J. I. Choi, J. R. Lee, and J. R. Youn, Polym. Polym. Compos. **18**, 381 (2010).